
Synthesis and evaluation of novel F-18 labeled quinazoline derivatives with low lipophilicity for tumor PET imaging

Yan Chong, Jin Chang, Wenwen Zhao, Yong He, Yuqiao Li, Huabei Zhang, and Chuanmin Qi*

Key Laboratory of Radiopharmaceuticals, College of Chemistry, Beijing Normal University, Beijing 100875, People's Republic of China

Corresponding Author: Tel. +86-136 8138 0097; Fax. +86-10-58802075;

E-mail: qicmin@sohu.com

ABSTRACT

Four novel F-18 labeled quinazoline derivatives with low lipophilicity, [¹⁸F]4-(2-fluoroethoxy)-6,7-dimethoxyquinazoline ([¹⁸F]I), [¹⁸F]4-(3-((4-(2-fluoroethoxy)-7-methoxyquinazolin-6-yl)oxy)propyl)morpholine ([¹⁸F]II), [¹⁸F]4-(2-fluoroethoxy)-7-methoxy-6-(2-methoxyethoxy)quinazoline ([¹⁸F]III) and [¹⁸F]4-(2-fluoroethoxy)-6,7-bis(2-methoxyethoxy)quinazoline ([¹⁸F]IV), were synthesized via a two-step radiosynthesis procedure with an overall radiochemical yield of 10-38% (without decay correction) and radiochemical purities of > 98%. The lipophilicity and stability of labeled compounds were tested in vitro. The log P values of the four radiotracers ranged from 0.52 to 1.07. We then performed ELISA to measure their affinities to EGFR-TK. ELISA assay results indicated that each inhibitor was specifically bound to EGFR-TK in a dose-dependent manner. The EGFR-TK autophosphorylation IC₅₀ values of [¹⁸F]I, [¹⁸F]II, [¹⁸F]III, and [¹⁸F]IV were 7.732 μM, 0.4698 μM, 0.1174 μM, and 0.1176 μM, respectively. All labeled compounds were evaluated via cellular uptake and blocking studies in HepG2 cell lines in vitro. Cellular uptake and

This article has been accepted for publication and undergone full peer review but has not been through the copyediting, typesetting, pagination and proofreading process which may lead to differences between this version and the Version of Record. Please cite this article as doi: 10.1002/jlcr.3538

blocking experiment results indicated that [^{18}F]I and [^{18}F]III had excellent cellular uptake at 120 min post-injection in HepG2 carcinoma cells (51.80 ± 3.42 %ID/mg protein and 27.31 ± 1.94 %ID/mg protein, respectively). Additionally, biodistribution experiments in S180 tumor-bearing mice in vivo indicated that [^{18}F]I had a very fast clearance in blood and a relatively high uptake ratio of tumor to blood (4.76) and tumor to muscle (1.82) at 60 min post-injection. [^{18}F]III had a quick clearance in plasma, and its highest uptake ratio of tumor to muscle was 2.55 at 15 min post-injection. These experimental results and experiences were valuable for the further exploration of novel radiotracers of quinazoline derivatives.

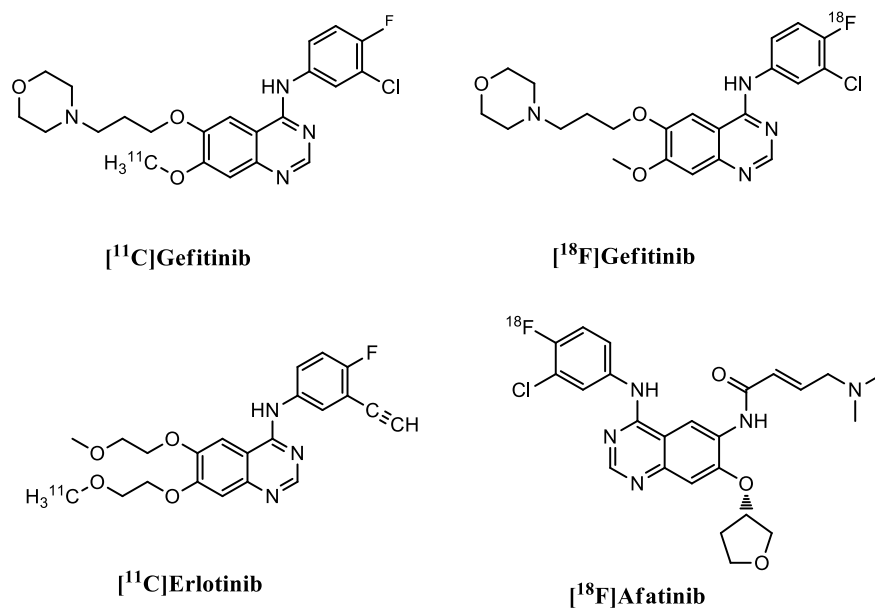
Key Words: fluoride-18; quinazoline derivatives; EGFR; PET imaging probes

1. Introduction

The epidermal growth factor receptor (EGFR) has been reported to be closely related to human tumor diseases¹. Nearly 80 percent of cancer cell lines have an over-expression of EGFR². The activation of EGFR by specific ligands could influence the RAS-ERK and PI3K-AKT signal transduction pathways¹. Consequently, this will cause abnormalities in cell division, proliferation, survival, apoptosis, migration and other biological reactions. Quinazoline derivative is one of EGFR tyrosine kinase inhibitor found in the early stage³. This type of small molecular inhibitor has outstanding specific binding affinities to EGFR and has attracted the attention of many researchers. Therefore, many EGFR tyrosine kinase inhibitors of quinazoline derivatives, such as Gefitinib^{4,5}, Erlotinib⁶, Lapatinib⁷, Vandetanib⁸, and Afatinib⁹, have been approved to be used for the treatment of cancer, especially non-small cell lung cancer (NSCLC), in recent decades.

With the rapid development of nuclear medical technology, positron emission tomography (PET) has become a noninvasive and reliable method with which to diagnose cancer¹⁰. Among positron nuclides, fluoride-18 has been favored as a medical PET nuclide for its convenient half-life (109.8 min) and emission energy (635 keV)^{11,12}. Moreover, researchers have tried to find appropriate F-18 labeled radiotracers to realize the accurate diagnosis of tumor diseases in an early stage. To date, the most successful and commonly used F-18 labeled tumor PET imaging probe is [¹⁸F]2-fluoro-2-deoxy-D-glucose ([¹⁸F]FDG)¹³, which has been used to reflect glucose metabolism in tumor cells. Many researchers have developed additional novel PET radiotracers for the diagnosis of specific tumor diseases, e.g., [¹⁸F]3'-deoxy-3'-fluorothymidine ([¹⁸F]FLT)^{14,15}, [¹⁸F]O-(2-fluoroethyl-L-tyrosine ([¹⁸F]FET)¹⁶, and [¹⁸F] fluoro-misonidazole ([¹⁸F]FMISO)¹⁷.

Due to the high affinity of quinazoline derivatives to over-expressed EGFR in tumor cell lines, researchers have attempted to design radioisotope labeled quinazoline derivatives as radiotracers to target EGFR for the diagnosis of tumor diseases¹⁸. [¹¹C]Gefitinib¹⁹, [¹¹C]Erlotinib²⁰, [¹⁸F]Gefitinib²¹⁻²³, [¹⁸F]Afatinib²⁰ and other tumor PET imaging probes of quinazoline derivatives have been developed and evaluated. However, these radiotracers encountered some drawbacks in PET imaging: low tumor uptake, poor solubility and high non-specific binding¹⁸. Therefore, we tried to develop novel F-18 labeled quinazoline derivatives in order to overcome these shortcomings.



Scheme 1 Structures of some radioisotope labeled quinazoline derivatives

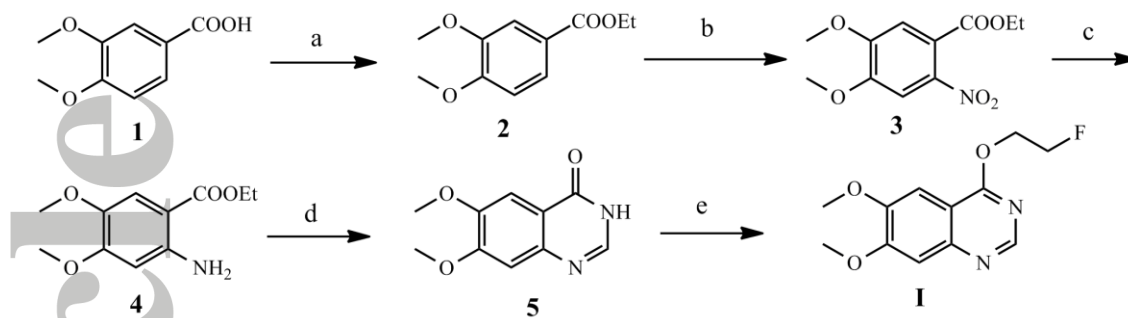
Helen Su et al. revealed the intrinsic reason for the poor PET imaging effect of F-18 labeled quinazoline derivatives with their research on [^{18}F]Gefitinib²⁴. They concluded that 4-anilinoquinazoline derivatives had rather high lipophilicity, which would result in considerable non-specific binding on the lipophilic cell membrane and low clearance in plasma. Consequently, the low uptake ratio of tumor to background would hinder the use of this type of probe as a promising PET imaging radiotracer due to the high lipophilicity. Enlightened by their thesis and conclusion, we attempted to improve the water solubility of quinazoline derivatives to decrease the non-specific binding in vivo and increase the clearance rate in plasma. Because the 4-anilino group severely influenced the lipophilicity of quinazoline derivatives, we replaced this group with a 2-fluoroethoxy group to increase the hydrophilicity. Although this substitution may weaken the specific binding ability of quinazoline derivatives to EGFR, we anticipate that our novel radiotracers will have a rapid clearance in plasma to increase the uptake ratio of tumor to background. Therefore, we finally designed and synthesized four F-18 labeled quinazoline derivatives: [^{18}F]4-(2-fluoroethoxy)-6,7-dimethoxyquinazoline (**[^{18}F]I**), [^{18}F]4-(3-((4-(2-fluoroethoxy)-7-methoxyquinazolin-6-

yl)oxy)propyl)morpholine ($[^{18}\text{F}]\text{II}$), $[^{18}\text{F}]4\text{-(2-fluoroethoxy)-7-methoxy-6-(2-methoxyethoxy)quinazoline}$ ($[^{18}\text{F}]\text{III}$) and $[^{18}\text{F}]4\text{-(2-fluoroethoxy)-6,7-bis(2-methoxyethoxy)quinazoline}$ ($[^{18}\text{F}]\text{IV}$). Then, we performed biological activity studies and evaluated these radiotracers rationally.

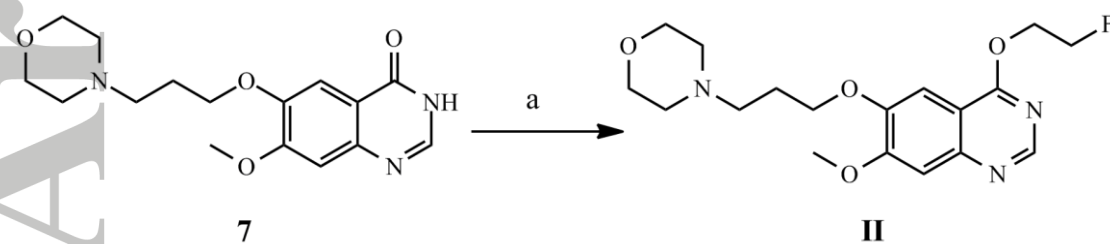
2. Results and Discussion

2.1. Chemistry

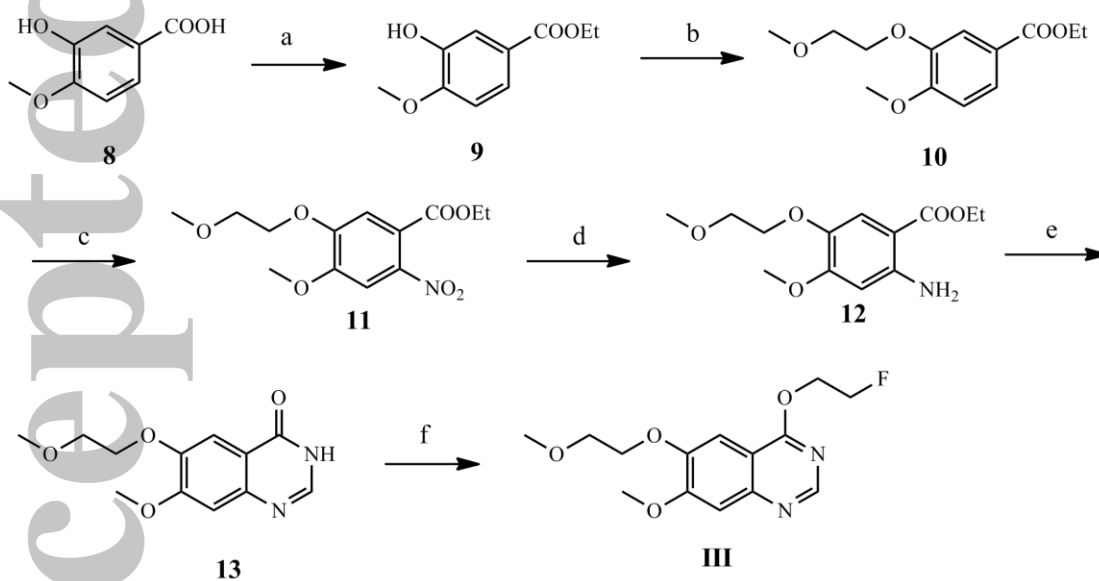
We referred to our previous article (Shilei Li et al.)²⁵ and simply optimized the synthesis methods of **I**, **II**, **III**, and **IV** (**Scheme 1-4**). Compound **I** was prepared through a five-step synthesis procedure as shown in **Scheme 1**. Compound **5** was obtained through a series of reactions that included esterification, nitration, hydrogenation reduction and cyclization with formamide. Compound **5** was the precursor of radiotracer $[^{18}\text{F}]\text{I}$. It was substituted by 2-fluoroethyl tosylate with K_2CO_3 as a base to produce compound **I**. The 2-fluoroethyl tosylate (Compound **6**) was prepared via the tosylation of 2-fluoroethanol with KOH as a strong base. Similarly, compound **II** was also obtained via a 2-fluoroethyl tosylate substitution with compound **7** (**Scheme 2**). Compounds **III** and **IV** were prepared in a similar fashion (**Scheme 3-4**). After the initial 1-bromo-2-methoxyethane substitution reaction, the remainder of the synthesis section was similar to the five-step synthesis method of compound **I**. The overall synthesis process could be finished efficiently with high yields and less purification. Precursors for radiosynthesis (Compounds **5**, **7**, **13**, **18**) could also be easily prepared with high yields.



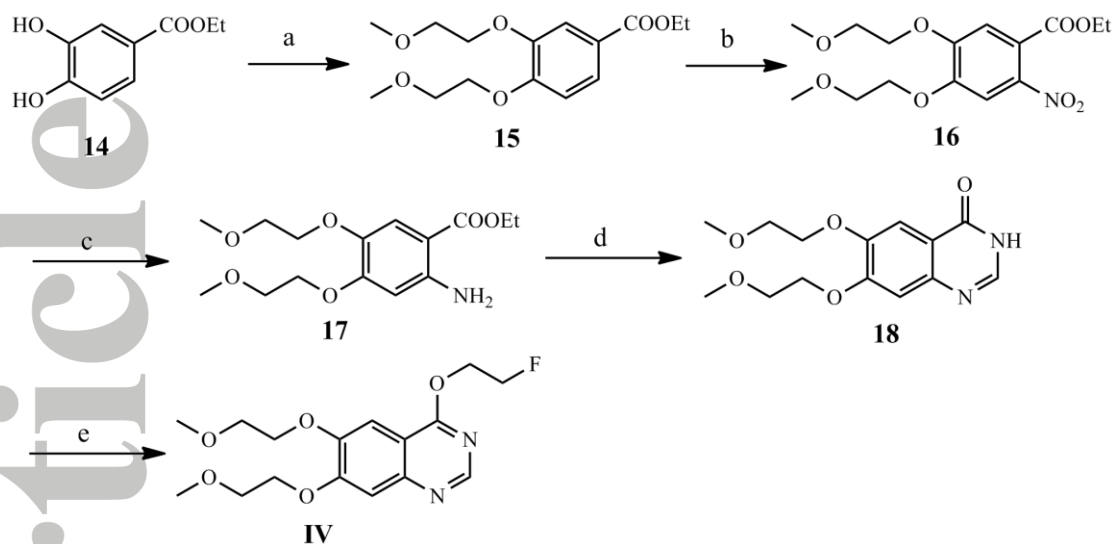
Scheme 2 Synthesis of compound I. Reagents and conditions: (a) EtOH, conc. H₂SO₄, Reflux; (b) 65% HNO₃, CH₃COOH, 0°C; (c) H₂, Pd/C, CH₃OH, 40°C; (d) HCONH₂, 160-170°C; (e) TsOCH₂CH₂F (Compound 6), DMF, K₂CO₃, 90-100°C.



Scheme 3 Synthesis of compound II. Reagents and conditions: (a) TsOCH₂CH₂F (Compound 6), DMF, K₂CO₃, 90-100°C.

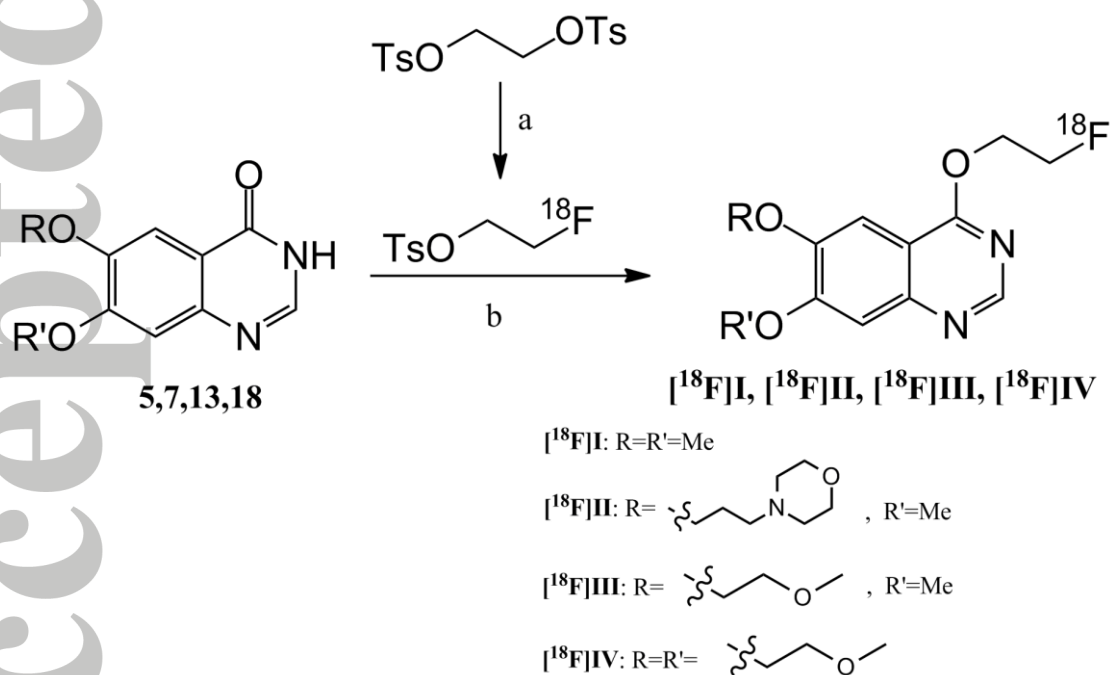


Scheme 4 Synthesis of compound III. Reagents and conditions: (a) CH₃CH₂OH, conc. H₂SO₄, Reflux; (b) CH₃OCH₂CH₂OBr, Bu₄NBr, K₂CO₃, CH₃CN, Reflux; (c) 65% HNO₃, CH₃COOH, 0°C; (d) H₂, Pd/C, CH₃OH, 40°C; (e) HCONH₂, 160-170°C; (f) TsOCH₂CH₂F, DMF, K₂CO₃, 90-100°C.



Scheme 5 Synthesis of compound IV. Reagents and conditions: (a) $\text{CH}_3\text{OCH}_2\text{CH}_2\text{OBr}$, Bu_4NBr , K_2CO_3 , CH_3CN , Reflux; (b) 65% HNO_3 , CH_3COOH , 0°C ; (c) H_2 , Pd/C , CH_3OH , 40°C ; (d) HCONH_2 , $160\text{-}170^\circ\text{C}$; (e) $\text{TsOCH}_2\text{CH}_2\text{F}$, DMF , K_2CO_3 , $90\text{-}100^\circ\text{C}$.

2.2. Radiochemistry



Scheme 6 Radiochemical synthesis of $^{18}\text{F}\text{I}$, $^{18}\text{F}\text{II}$, $^{18}\text{F}\text{III}$, and $^{18}\text{F}\text{IV}$. Reagents and conditions: (a) $\text{K}^{18}\text{F}/\text{K}_{2.2.2}$, anhydrous CH_3CN , K_2CO_3 , 100°C , 15 min; (b) Anhydrous DMF , K_2CO_3 , 100°C , 15-30 min.

All radiotracers were prepared with the [^{18}F]KF-K_{2.2.2} complex via the same two-step labeling procedure as shown in **Scheme 5**. The procedure included nucleophilic fluorosubstitution of glycol-1,2-ditosylate and the substitution of 2- [^{18}F]fluoroethyl tosylate with precursors (Compounds **5**, **7**, **13**, **18**). The radiosynthesis procedure, including HPLC separation, could be finished within 90 min. The overall radioactivity yield of these four labeled products without decay correction was approximately 10%-38% and radiochemical purities were all above 98%. The molar activity of four labeled compounds ranged from 61.0-69.5 GBq/ μmol . All related HPLC data and RCY of [^{18}F]I, [^{18}F]II, [^{18}F]III, and [^{18}F]IV are summarized in **Table 1**.

Table 1. Retention time, HPLC conditions and overall radioactivity yield of I, II, III, and IV.

Compounds	Retention Time (min)	Radio-HPLC Conditions (solvent, flow rate)	The Overall Radioactivity Yield*
[^{18}F]I	11.4	CH ₃ OH:H ₂ O=60:40[v:v], 2 mL/min	28.1%
[^{18}F]II	13.6	same as above	10.9%
[^{18}F]III	11.8	same as above	37.9%
[^{18}F]IV	12.8	same as above	36.7%

*Without decay correction

2.3. Stability in vitro

The radio-HPLC analysis results indicated that all labeled compounds were stable for at least 2 hours in bovine serum at 37°C without radioautolysis. Related radio-HPLC of labeled compounds is shown in the supplemental materials.

2.4. Partition Coefficients

Partition coefficients (log P) of the four labeled compounds are shown in **Table 2**. The log P values of the four radiotracers ranged from 0.52 to 1.07. Compared with the log P value of

[¹⁸F]Gefitinib (3.46) reported in related article²⁴, all labeled compounds had noticeably decreased lipophilicity as we expected.

Table 2. Partition coefficient values of [¹⁸F]I, [¹⁸F]II, [¹⁸F]III, and [¹⁸F]IV (log P value, mean±SD, n=3).

Compound	Partition coefficient (log P)
[¹⁸ F]I	1.07±0.03
[¹⁸ F]II	0.52±0.02
[¹⁸ F]III	0.97±0.02
[¹⁸ F]IV	0.80±0.07

2.5 ELISA

We performed ELISA to evaluate biological activities of target compounds. We also selected Gefitinib as a comparative inhibitor of EGFR-TK in this experiment. The blocking rate-dose curves and IC₅₀ values of inhibitors of EGFR-TK are shown in **Figure 1** and **Table 3**, respectively.

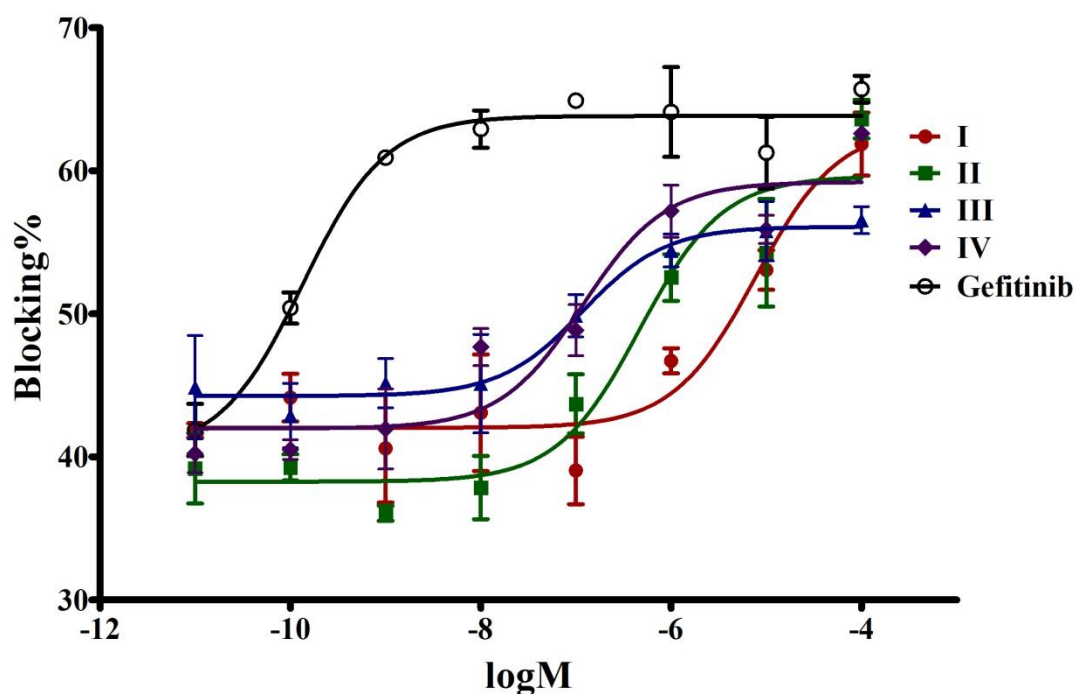


Figure 1. Blocking rate-inhibitor dose curves of ELISA (n=4): red line: I, green line: II, blue line: III, purple line: IV, and black line: Gefitinib

Table 3. The IC₅₀ values of inhibitors of EGFR tyrosine kinase (95% confidence interval is shown in parentheses, n=4).

Inhibitor	IC ₅₀ value of EGFR-TK autophosphorylation (mol/L)	
I	7.732×10 ⁻⁶	(3.246×10 ⁻⁶ -1.842×10 ⁻⁵)
II	4.698×10 ⁻⁷	(2.011×10 ⁻⁷ -1.097×10 ⁻⁶)
III	1.174×10 ⁻⁷	(4.577×10 ⁻⁸ -3.013×10 ⁻⁷)
IV	1.176×10 ⁻⁷	(4.806×10 ⁻⁸ -2.875×10 ⁻⁷)
Gefitinib	1.347×10 ⁻¹⁰	(7.802×10 ⁻¹¹ -2.325×10 ⁻¹⁰)

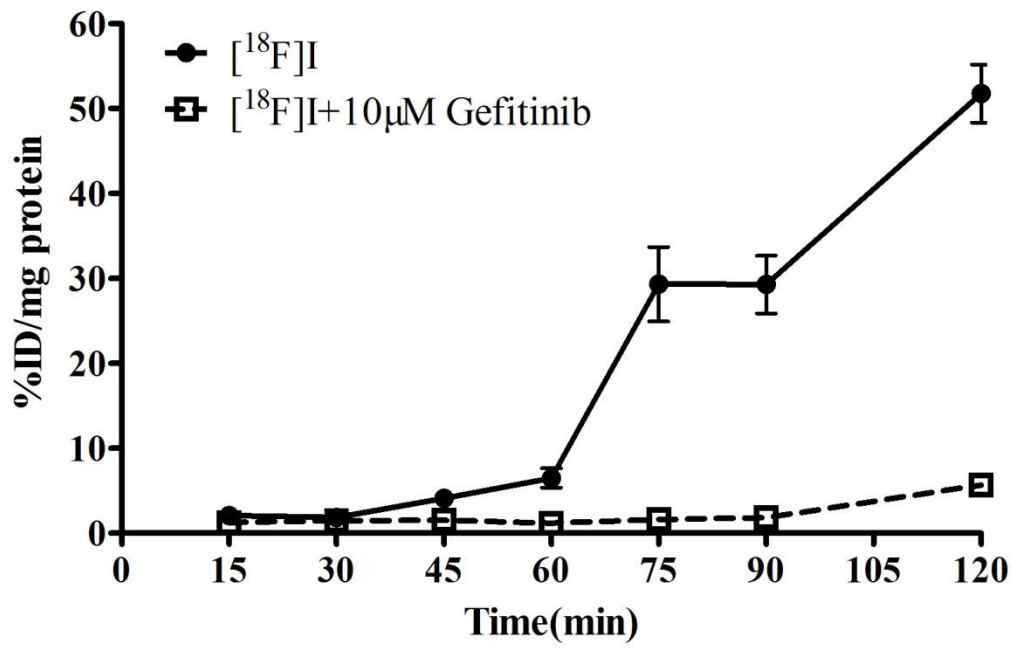
Generally, the blocking rate of all inhibitors appeared to be dose-dependent. The results also demonstrated that all inhibitors were specifically bound to EGFR-TK. The IC₅₀ values of EGFR-TK autophosphorylation for compounds **I**, **II**, **III** and **IV** were 7.732 μM, 0.4698 μM, 0.1174 μM, and 0.1176 μM, respectively. The four inhibitors without a 4-anilino group on the quinazoline ring still retained specific binding abilities to the target receptor to some extent. However, their affinities for EGFR-TK were lower than that of Gefitinib, which had an IC₅₀ value of 0.1347 nM. This finding indicated that the 4-anilino group on quinazoline derivatives made a significant contribution to the specific binding to EGFR-TK. Replacing the anilino group with a 2-fluoroethoxy group would sacrifice the inhibitor's affinity to EGFR. However, we were searching for quinazoline derivatives with low lipophilicity, which could make them to have a faster clearance rate in the blood and less non-specific binding. We had to make this change though it would actually lead to a decreased affinity for the receptor.

Compound **III** had the lowest IC₅₀ value of EGFR-TK autophosphorylation among the four inhibitors we synthesized. Compound **IV** had nearly the same biological activity as compound **III**. This result indicated that replacing methoxy with 2-methoxyethoxy at the C-7 position of quinazoline hardly influenced the affinity of 4-(2-fluoroethoxy)-quinazoline derivatives. However, the substituent group at the C-6 position of quinazoline could influence

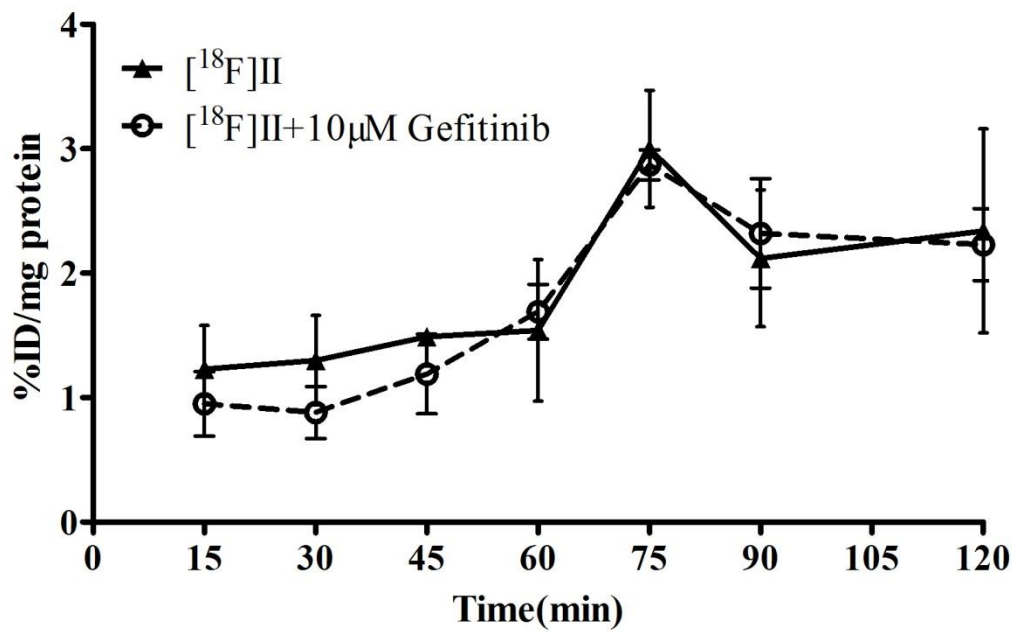
the IC₅₀ value. Compounds **I** and **II** were less potent than compound **III**. We supposed that the length of the substituent group at the C-6 position should not be too long or too short. The lipophilicity of the substituent group at the C-6 position was irrelevant to the affinity of 4-(2-fluoroethoxy)-quinazoline derivatives.

2.6. Cellular Uptake and Blocking Studies

Accepted Article

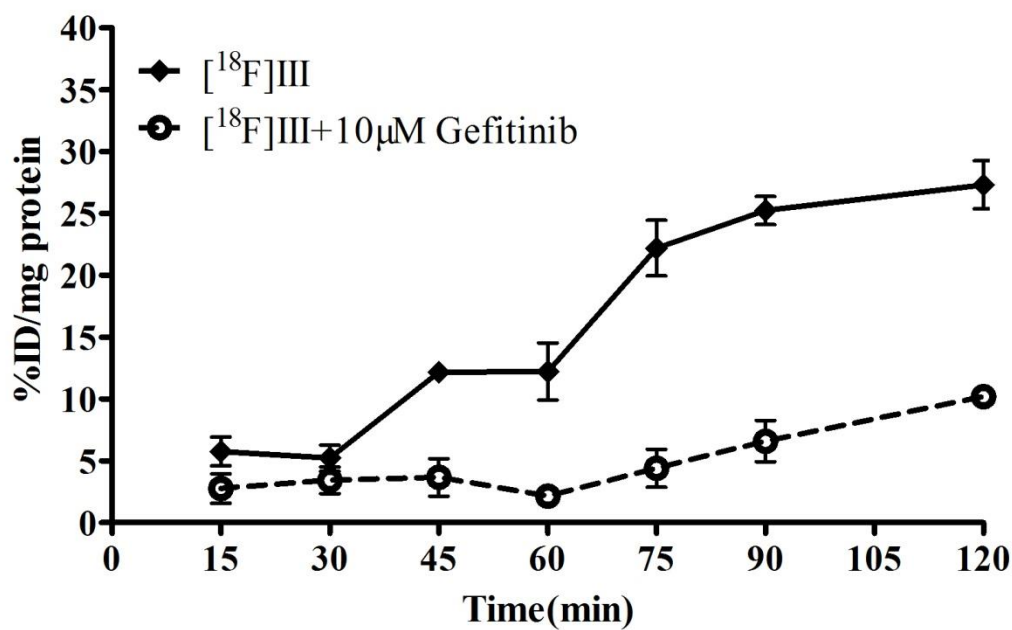


a

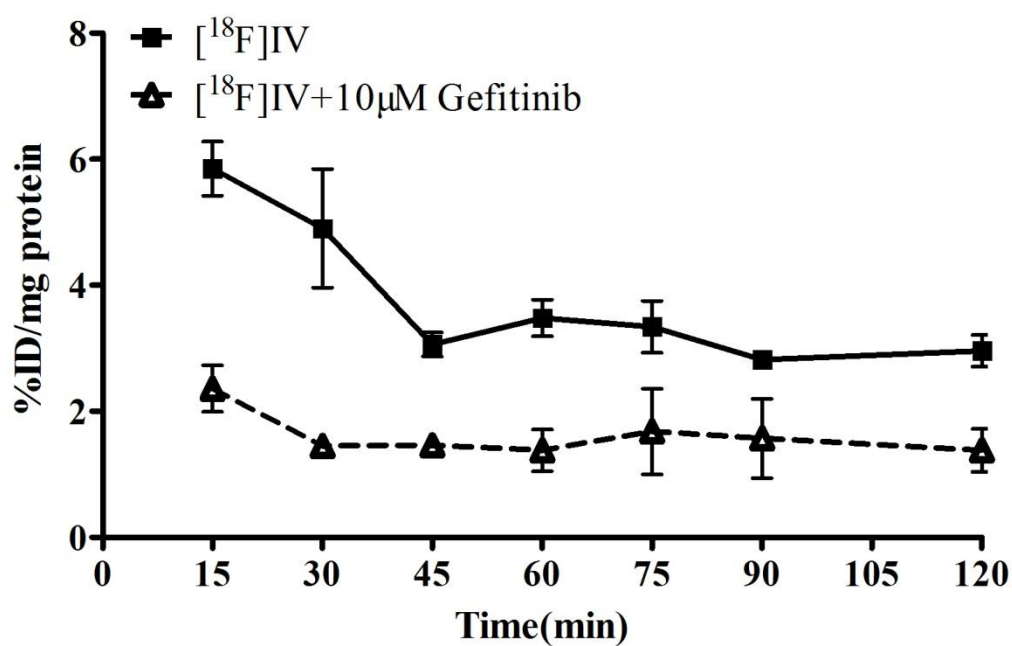


b

AC



c



d

Figure 2. Cellular uptake and blocking studies of the radiotracers $[^{18}\text{F}]\text{I}$ (a), $[^{18}\text{F}]\text{II}$ (b), $[^{18}\text{F}]\text{III}$ (c) and $[^{18}\text{F}]\text{IV}$ (d) in HepG2 human hepatocellular carcinoma cells (n=4).

The cellular uptake and blocking studies were performed in HepG2 human hepatocellular carcinoma cells, which had a medium level of EGFR over-expression. According to the cellular uptake results of each labeled compound (**Figure 2a-d**), [^{18}F]I and [^{18}F]III noticeably increased uptake in 2 hours. The highest cellular uptake values of [^{18}F]I and [^{18}F]III were 51.80 ± 3.42 %ID/mg and 27.31 ± 1.94 %ID/mg protein, respectively, at 120 min. [^{18}F]I and [^{18}F]III had excellent cellular association with HepG2 cell lines. In contrast, [^{18}F]IV showed a declining trend in cellular uptake as time elapsed. The highest cellular uptake value was only 5.85 ± 0.43 %ID/mg protein within the first 15 min. We supposed that [^{18}F]IV had better hydrophilicity and, therefore, did not penetrate the lipophilic cell membrane well. Additionally, [^{18}F]IV had poor stability in organisms according to the latter result of the biodistribution experiment. These potential factors resulted in a decreased cellular uptake of [^{18}F]IV. Similarly, [^{18}F]II had the weakest cellular uptake because it had the lowest lipophilicity.

According to blocking experiments results, compounds [^{18}F]I, [^{18}F]III and [^{18}F]IV significantly reduced cellular uptake when they were incubated with 10 μM Gefitinib, an EGFR tyrosine kinase inhibitor. The blocking percentages of Gefitinib to these three radiotracers were often over 50%. This finding indicated that Gefitinib had a competitive relationship with [^{18}F]I, [^{18}F]III and [^{18}F]IV in terms of cellular association. To some extent, it also demonstrated that [^{18}F]I, [^{18}F]III and [^{18}F]IV bound specifically to EGFR in HepG2 carcinoma cells. However, we did not observe an obvious decline in the cellular uptake of [^{18}F]II when it was incubated with a 10 μM inhibitor. The cellular uptake value changed slightly and was maintained at a very low level, which suggested that [^{18}F]II had high non-specific binding to EGFR in HepG2 cells. We concluded that [^{18}F]II had the lowest lipophilicity (log P=0.52), which hindered the ability of the molecule to reach the target receptor inside of cell membrane and resulted in a high non-specific cellular association.

2.7. Biodistribution in S180 Tumor-Bearing Mice

Table 3. Biodistribution data of [¹⁸F]I in S180 tumor-bearing mice (%ID/g, mean±SD, n=4).

Organ	5 min	15 min	30 min	60 min	120 min
Blood	5.31±0.07	2.27±1.03	1.45±0.44	0.23±0.05	0.58±0.18
Heart	3.47±0.45	2.15±0.06	1.13±0.23	1.10±0.29	0.28±0.07
Liver	6.02±0.92	2.06±0.79	0.84±0.25	0.65±0.19	0.11±0.02
Spleen	2.62±0.46	0.89±0.59	0.74±0.33	0.39±0.04	0.17±0.09
Lung	4.20±0.83	1.46±0.59	0.92±0.29	0.70±0.26	0.25±0.06
Kidney	11.90±2.13	4.95±2.15	1.49±0.61	1.07±0.33	0.37±0.05
Intestine	2.35±0.27	5.92±2.74	7.55±1.11	2.28±1.43	0.74±0.33
Stomach	2.15±0.68	0.30±0.11	0.82±0.10	0.48±0.23	0.21±0.08
Bone	1.88±0.33	0.93±0.49	2.75±0.12	1.89±0.74	1.86±0.88
Muscle	2.83±0.52	0.87±0.56	1.15±0.15	0.60±0.09	0.66±0.31
Brain	1.50±0.64	0.53±0.26	0.70±0.25	0.75±0.36	0.18±0.10
Tumor	3.26±0.12	1.58±1.12	1.82±0.04	1.09±0.31	0.52±0.06
Tumor/Muscle	1.15	1.81	1.59	1.82	0.79
Tumor/Blood	0.61	0.70	1.26	4.76	0.90

Table 4. Biodistribution data of [¹⁸F]II in S180 tumor-bearing mice (%ID/g, mean±SD, n=4).

Organ	5 min	15 min	30 min	60 min	120 min
Blood	2.30±0.68	1.51±0.31	1.28±0.18	0.81±0.17	0.52±0.05
Heart	3.36±1.06	1.86±0.61	1.49±0.31	0.92±0.20	0.51±0.10
Liver	10.03±2.94	9.45±0.07	6.61±0.27	3.28±0.35	1.53±0.60
Spleen	5.89±1.55	4.90±0.06	2.29±0.63	1.08±0.51	0.49±0.12
Lung	4.38±1.11	4.90±0.46	1.47±0.27	1.05±0.31	0.58±0.05
Kidney	7.77±2.02	4.60±1.10	3.35±0.49	1.62±0.55	1.39±0.26
Intestine	2.40±0.83	7.53±2.64	9.28±2.44	20.77±0.57	31.79±1.57
Stomach	8.72±0.69	8.52±0.92	11.09±0.37	4.43±2.29	1.41±0.18
Bone	2.47±1.23	4.07±0.81	2.40±1.29	2.40±1.41	3.45±0.25
Muscle	2.61±0.87	1.56±0.23	1.22±0.32	0.76±0.19	0.43±0.12
Brain	0.58±0.28	0.38±0.14	0.34±0.04	0.24±0.06	0.26±0.09
Tumor	1.56±1.09	1.87±0.39	1.90±0.27	1.06±0.30	0.92±0.11
Tumor/Muscle	0.60	1.20	1.56	1.40	2.14
Tumor/Blood	0.83	1.24	1.49	1.31	1.76

Table 5. Biodistribution data of [¹⁸F]III in S180 tumor-bearing mice (%ID/g, mean±SD, n=4).

Organ	5 min	15 min	30 min	60 min	120 min
Blood	2.93±0.43	1.77±0.27	1.18±0.11	1.12±0.05	0.68±0.13
Heart	2.41±0.06	1.58±0.30	1.24±0.11	1.01±0.23	0.73±0.24
Liver	2.95±0.72	1.24±0.61	1.00±0.12	0.46±0.02	0.44±0.36
Spleen	1.61±0.18	1.03±0.25	0.74±0.11	0.51±0.06	0.46±0.13
Lung	3.12±0.35	1.68±0.20	5.32±0.16	1.76±0.02	1.74±0.09
Kidney	3.13±1.36	1.82±0.59	1.22±0.15	0.68±0.16	0.49±0.10
Intestine	1.83±0.07	3.30±0.53	4.95±0.10	2.12±0.22	1.10±0.64
Stomach	1.47±0.27	1.67±0.52	0.68±0.14	1.80±1.14	0.46±0.14
Bone	2.21±0.50	1.52±0.80	1.98±0.43	1.93±1.33	1.74±0.67
Muscle	1.87±0.15	0.87±0.27	0.84±0.13	0.86±0.14	0.45±0.09

Brain	1.03±0.18	0.76±0.14	0.63±0.08	0.44±0.13	0.45±0.11
Tumor	2.05±0.20	2.23±0.49	1.52±0.06	1.22±0.32	0.94±0.17
Tumor/Muscle	1.10	2.55	1.81	1.43	2.08
Tumor/Blood	0.70	1.25	1.29	1.09	1.31

Table 6. Biodistribution data of [¹⁸F]IV in S180 tumor-bearing mice (%ID/g, mean±SD, n=4).

Organ	5 min	15 min	30 min	60 min	120 min
Blood	3.94±0.66	4.03±0.58	3.23±0.12	3.56±0.32	1.81±0.14
Heart	3.16±0.98	3.39±0.14	3.08±0.18	3.33±0.45	1.69±0.44
Liver	2.32±0.62	3.35±0.75	2.34±0.46	2.08±0.81	1.63±0.19
Spleen	3.01±0.47	2.29±1.09	2.30±0.04	2.04±0.69	1.28±0.24
Lung	3.36±1.13	3.23±0.47	4.14±0.53	3.11±0.35	2.75±0.61
Kidney	3.51±0.25	2.71±0.50	1.89±0.65	2.12±0.25	1.31±0.22
Intestine	3.70±0.30	2.62±1.09	2.97±0.47	3.73±1.25	1.61±0.07
Stomach	1.94±0.55	2.55±0.71	1.35±0.17	1.62±0.46	0.96±0.33
Bone	2.57±1.09	3.35±0.34	2.87±0.67	8.54±2.86	10.31±0.88
Muscle	2.47±0.75	2.49±0.55	2.43±0.15	1.93±0.32	1.65±0.21
Brain	1.20±0.24	1.92±0.04	1.86±0.13	2.10±0.28	1.22±0.14
Tumor	3.43±0.50	3.52±0.14	4.07±1.13	4.47±0.58	2.64±0.30
Tumor/Muscle	1.39	1.41	1.67	2.32	1.60
Tumor/Blood	0.87	0.87	1.26	1.26	1.46

The biodistribution experiments of all radiotracers were executed in S180 tumor-bearing mice. According to the biodistribution data summarized in **Table 3-6**, all radiotracers had high initial uptake in the kidney and liver, which then quickly decreased as time elapsed. In addition, we observed an obvious accumulation in the intestine. Nearly all other organs and tissues had the highest uptake 5 min after the injection, which then consecutively declined as time passed.

[¹⁸F]I had the highest tumor uptake (3.26±0.12 %ID/g) during the initial 5 min, and then, [¹⁸F]I cleared quickly as time passed. Although this radiotracer did not have an accumulation process in the tumor, it actually had a much faster clearance rate in blood than in the tumor so that it could have a relatively high tumor to blood ratio (approximately 4.76) at 60 min post-injection. The tumor to muscle uptake ratio value was highest (1.82) at the same time. In conclusion, 60 min post-injection should be the best imaging time of [¹⁸F]I. This compound has the potential to be an EGFR targeted tumor radiotracer.

In contrast to [^{18}F]I, we found that [^{18}F]II accumulated in the tumor. The maximum uptake value of [^{18}F]II was 1.90 ± 0.27 %ID/g at 30 min post-injection. Compared with [^{18}F]I, the lower lipophilicity of [^{18}F]II did not contribute to an increase in clearance rate in the blood but diminished tumor absorption. The uptake ratios of tumor to muscle and tumor to blood were often less than 2, which suggested that [^{18}F]II was not suitable as a PET tumor imaging probe.

[^{18}F]III had a maximum uptake value of 2.23 ± 0.49 %ID/g at 15 min post-injection and the tumor uptake remained above 1.50 %ID/g in the initial 30 min. However, the uptake in the tumor was low due to the increased hydrophilicity. The clearance of [^{18}F]III in blood was quite fast so that the uptake ratio of tumor to blood remained steady 15 min post-injection. The highest uptake ratio of tumor to muscle was 2.55 at 15 min post-injection. Therefore, the 15 min post-injection time point should be appropriate for tumor imaging.

For the radiotracer [^{18}F]IV, we observed that the bone uptake of [^{18}F]IV noticeably increased as time elapsed. This result indicated that the [^{18}F]IV radiotracer had severe defluorination in vivo. The accumulation of free fluoride-18 in bones led to an increase in radioactivity. However, the reason why only [^{18}F]IV had severe defluorination in vivo is unknown. Propose that a substitution group at the C-7 position had an influence on the molecular stability or metabolism in vivo. Although [^{18}F]IV had the highest tumor uptake value among all four labeled compounds, it could not serve as a tumor imaging probe due to poor stability in vivo.

3. Experimental Section

3.1 General

All chemical reagents and solvents were commercially available. Cell culture medium, other related biological evaluation and experimental reagents and kits were purchased from Yeasen Biological Inc in Shanghai. No-carrier-added fluoride-18 was provided by the PET Center of Xuanwu Hospital and The General Hospital of the People's Liberation Army via the $^{18}\text{O}(\text{p}, \text{n})^{18}\text{F}$ nuclear reaction. Semi-preparative HPLC reversed-phase columns (C18 column, 250×10 mm, particle size: 10 μm) were purchased from Agela™ Venusil. HPLC separation was carried out on a Shimadzu™ LC-20A High-Performance Liquid Chromatography system. C18 Sep-Pak Cartridges were purchased from Waters™ and activated with 2 mL of methanol and 2×10 mL of water before use. Melting points were measured in capillary tubes with an RY-1 melting point apparatus and were uncorrected. Nuclear magnetic resonance spectra (^1H and ^{13}C -NMR) were performed on a Bruker™ spectrometer (400 MHz for ^1H -NMR and 100 MHz for ^{13}C -NMR), and chemical shifts (δ values, ppm) were reported downfield from TMS. Mass spectra were measured with a Bruker™ Apex IV FTM instrument using a low-resolution electrospray ionization (ESI) source at the Mass Spectroscopy Center of Beijing Normal University. The radioactive counts were measured with a Wizard™ 1470 Gamma Counter, and the radioactivities were obtained via an RM-905a Radioactivity Meter. HepG2 hepatocellular carcinoma cells were purchased from the Cancer Hospital of the Chinese Academy of Medical Science and cultured in DMEM (including 10% FBS) in 5% CO_2 atmosphere at 37°C. The ICR mice were supported by the Experimental Animal Department of Peking University Health Science Center.

3.2. Synthesis

The synthesis methods of the intermediate products (Compounds **1-18**) are described in a related reference²⁵. The target compounds' chemical synthesis method and ¹H-NMR, ¹³C-NMR and MS data of target compounds are shown as below. Related spectra are shown in the supplemental data.

Preparation of 4-(2-fluoroethoxy)-6,7-dimethoxyquinazoline (I). Compound **5** (206 mg, 1.0 mmol) and compound **6** (432 mg, 2.0 mmol) were added to 5 mL of DMF. The reaction solution was stirred at 90-100°C for 2 hours. The solution was poured into 50 mL of ice water under stirring and then extracted with 10 mL of ethyl acetate (10mL×8). The organic layer was washed with saturated NaHCO₃ solution (10 mL×1), saturated NaCl solution (10 mL×1) and distilled water (10 mL×2) in sequence and dried with Na₂SO₄. The solvent was removed under vacuum conditions to obtain a light yellow solid. The crude product was recrystallized from ethyl acetate and petroleum ether (v:v=3:1) to yield a light yellow target product (45 mg, 18% yield). m.p. 168-169°C. ¹H NMR (400 MHz, CDCl₃) δ 8.00 (s, 1H, ArH), 7.63 (s, 1H, ArH), 7.14 (s, 1H, ArH), 4.77 (dt, *J*= 47.2 Hz, 4.4 Hz, 2H, -CH₂-), 4.33 (dt, *J*=27.2 Hz, 4.4 Hz, 2H, -CH₂-), 4.03 (s, 6H, -OCH₃). ¹³C NMR (100 MHz, CDCl₃) δ 160.94 (s), 155.57 (s), 149.98 (s), 146.01 (s), 145.06 (s), 115.86 (s), 108.51 (s), 105.98 (s), 81.75 (d, *J*=168.8 Hz), 56.846 (s), 47.71 (d, *J*=19.5 Hz). MS (ESI⁺) *m/z*: 253.09 [M+H]⁺.

Preparation of 4-(3-((4-(2-fluoroethoxy)-7-methoxyquinazolin-6-yl)oxy)propyl)-morpholine (II). The synthesis method of compound **II** was similar to the preparation procedure of compound **I**. The initial compound **7** (0.319 g, 1.0 mmol) was commercially available. Additionally, the product could be recrystallized from methanol to afford pure product as a white solid (100 mg, 27% yield). m.p. 127-128°C. ¹H NMR (400 MHz, CDCl₃) δ 7.89 (s, 1H, ArH), 7.55 (s, 1H, ArH), 7.03 (s, 1H, ArH), 4.67 (dt, *J*=47.1 Hz, 4.4 Hz, 2H, -CH₂-), 4.22 (dt,

$J=27.2$ Hz, 4.6 Hz, 2H , $-\text{CH}_2-$), 4.13 (m, $J=6.72$ Hz, 2H , $-\text{CH}_2-$), 3.90 (s, 3H , $-\text{OCH}_3$), 3.65 (s, 4H , $-\text{CH}_2-$), 2.47 (m, $J=6.6$ Hz, 2H , $-\text{CH}_2-$), 2.38 (d, $J=7.24$ Hz, 4H , $-\text{CH}_2-$), 2.00 (m, $J=6.88$ Hz, 4H , $-\text{CH}_2-$). ^{13}C NMR (100 MHz, CDCl_3) δ 160.96 (s), 155.86 (s), 149.41 (s), 145.95 (s), 144.95 (s), 115.80 (s), 108.59 (s), 107.10 (s), 81.75 (d, $J=168.8$ Hz), 67.49 (s), 56.79 (s), 55.86 (s), 54.24 (s), 54.24 (s), 47.70 (d, $J=19.5$ Hz), 26.61 (s). MS (ESI⁺) m/z : 366.16 [M+H]⁺.

Preparation of 4-(2-fluoroethoxy)-7-methoxy-6-(2-methoxy-ethoxy)quinazoline (III). The synthesis method of compound **III** was similar to the preparation procedure of compound **I**. The product was recrystallized from methanol to yield a cotton-like yellow solid (112 mg, 33% yield), m.p. 141 - 142°C . ^1H NMR (400 MHz, CDCl_3) δ 7.89 (s, 1H , ArH), 7.54 (s, 1H , ArH), 7.03 (s, 1H , ArH), 4.66 (dt, $J=47.1$ Hz, 4.4 Hz, 2H , $-\text{CH}_2-$), 4.26 (m, $J=4.6$ Hz, 1H , $-\text{CH}_2-$), 4.20 (m, $J=4.6$ Hz, 3H , $-\text{CH}_2-$), 3.90 (s, 1H , $-\text{OCH}_3$), 3.77 (m, $J=3.84$ Hz, $-\text{CH}_2-$), 3.39 (s, 3H , $-\text{OCH}_3$). ^{13}C NMR (100 MHz, CDCl_3) δ 160.92 (s), 155.97 (s), 146.04 (s), 145.95 (s), 145.19 (s), 115.70 (s), 108.64 (s), 107.28 (s), 81.75 (d, $J=168.7$ Hz), 71.14 (s), 68.98 (s), 59.76 (s), 56.76 (s), 47.70 (d, $J=19.5$ Hz). MS (ESI⁺) m/z : 297.1 [M+H]⁺.

Preparation of 4-(2-fluoroethoxy)-6,7-bis(2-methoxyethoxy)quinazoline (IV). The synthesis method of compound **IV** was similar to the preparation procedure of compound **I**. The product was recrystallized from methanol to yield a white solid (56 mg, 16% yield). m.p. 118 - 119°C . ^1H NMR (400 MHz, CDCl_3) δ 7.89 (s, 1H , ArH), 7.54 (s, 1H , ArH), 7.03 (s, 1H , ArH), 4.66 (dt, $J=47.1$ Hz, 4.4 Hz, 2H , $-\text{CH}_2-$), 4.26 (s, 1H , $-\text{CH}_2-$), 4.18 (m, $J=4.72$ Hz, 5H , $-\text{CH}_2-$), 3.76 (m, $J=4.8$ Hz, 4H , $-\text{CH}_2-$), 3.39 (s, 6H , $-\text{OCH}_3$). ^{13}C NMR (100 MHz, CDCl_3) δ 160.90 (s), 155.28 (s), 146.04 (s), 145.93 (s), 146.01 (s), 145.07 (s), 115.94 (s), 109.83 (s), 107.86 (s), 81.76 (d, $J=168.7$ Hz), 71.08 (s), 69.10 (s), 59.87 (s), 47.70 (d, $J=19.5$ Hz). MS(ESI⁺) m/z : 341.13 [M+H]⁺.

3.3. Radiosynthesis

All radiotracers were prepared via the following labeling procedure. [^{18}F]fluoride, which was generated from the $^{18}\text{O}(\text{p}, \text{n})^{18}\text{F}$ nuclear reaction, was captured by a QMA anion exchange cartridge. Then, 4-8 mg $\text{K}_{2.2.2}$ cryptate and 6-8 mg potassium carbonate were dissolved in a mixture of the solvent of 1 mL acetonitrile and 0.5 mL water. The fluoride-18 anion was recovered by eluting the QMA anion exchange cartridge with the mixture solution. The solvent was azeotroped under a nitrogen stream at 110-120°C to dry the mixture. This drying process was repeated no fewer than three times. A total of 1 mL of anhydrous acetonitrile supplement was added into the vial after drying each time. Then, 2-4 mg of the initial compound, glycol-1,2-ditosylate, was reacted with the [^{18}F]KF- $\text{K}_{2.2.2}$ cryptate complex and potassium carbonate at 100°C for 15 min in anhydrous acetonitrile solvent to yield 2- [^{18}F]fluoroethyl tosylate. When the reaction was finished and the acetonitrile solvent was evaporated, 1-2 mg of purified precursor (Compound **5**, **7**, **13**, **18**) dissolved in anhydrous DMF was co-heated with newly prepared 2- [^{18}F]fluoroethyl tosylate at 100°C for 15-30 min. The reaction mixture was diluted with water and then passed through a C18 Sep-Pak cartridge. After eluting with 10 mL of water to wash out excess radioactive fluoride, the cartridge was finally eluted with 2 mL of acetonitrile to gather the labeled product. The product solution was finally purified with a reversed-phase HPLC C18 Column (Agela™ Venusil, 250×10 mm, particle size: 10 μm , $\text{CH}_3\text{OH}:\text{H}_2\text{O}=60:40[\text{v}:\text{v}]$, 2 mL/min) to separate the desired F-18 labeled product at the retention time. The retention time of the four labeled compound could refer to Table 1.

3.4. Plasma Stability Studies

The stability of all labeled compounds was tested by HPLC analysis via the same method. A solution of the labeled product in saline (approximately 100 μCi) was incubated in 1 mL of

bovine serum for 2 h at 37°C. Then, the plasma was centrifuged for 3 min at 1000 rpm. The supernatant was passed through a 0.22- μ m filter membrane and the stability of the product was analyzed via radio-HPLC with a reversed-phase HPLC C18 Column (Agela™ Venusil, 250 \times 10 mm, particle size: 10 μ m, CH₃OH:H₂O=60:40[v:v], 2 mL/min).

3.5. Partition Coefficients

The partition coefficients (log P) were measured via the following procedure. The log P value was determined by the radioactivity of 1-octanol and PBS (0.01 M, pH 7.2-7.4) at the same volume. Initially, 0.1 mL of the labeled compound (approximately 30-50 μ Ci) saline solvent was added to 1.9 mL PBS. Then, 2 mL of a water phase solution was mixed with 2 mL of 1-octanol. The mixture solution was centrifuged for 5 min at 1000 rpm. After the partition equilibrium, 0.2 mL of solution in the water and oil phase was collected to measure the radioactivity with a gamma counter. The log P value was calculated by the following formula: $\log P = \log[(\text{CPM}(n\text{-octanol}) - \text{CPM}(\text{background})) / (\text{CPM}(\text{PBS}) - \text{CPM}(\text{background}))]$.

3.6. ELISA

The ELISA was carried out based on the following procedure. A Corning 96-well plate was first coated with 0.01 M PBS diluted Poly(Glu:Tyr) 4:1 peptide solution at 37°C for 24 h. Then, the solution was removed and the plate was washed with 0.01 M PBST (containing 0.05% Tween 20) 3 times. After the plate was dry, 1 μ L of different concentrations of inhibitor solutions (ranging from 10⁻² to 10⁻⁹ M) were added. Then 49 μ L of 1 μ M ATP's HEPES-MnCl₂ buffer solution was added to each well. Ten minutes later, 50 μ L of 10 ng/mL recombinant human EGFR HEPES buffer solution was added to each well to activate the phosphorylation reaction. The plate was shaken under 37°C for 2 h. When the reaction was finished, the reaction solutions were removed and the plate was washed. A total of 100 μ L of

0.01 M PBST (including 0.5% BSA and 0.05% Tween 20) with P-Tyr-100 mouse mAb (1:1000) solution was added to the wells and reacted at 37°C. Forty-five minutes later, all solutions were removed and the plate was washed again. Then, 100 µL of 0.01 M PBST (including 0.5% BSA and 0.05% Tween 20) with diluted goat-anti-mouse peroxidase conjugated antibody (1:1000) solution was added. The reaction was stopped by washing as the previous step. Finally, 100 µL of *o*-phenylenediamine working solution (diluted with pH 5.4 citrate buffer) was added to each well and reacted for 30 minutes in the darkness. 50 µL of 2 M H₂SO₄ was added to each well to stop the chromogenic reaction, and the OD value of each well was measured with a microplate reader at 490 nm. The blocking rate (%) of specific concentrations of the inhibitor was calculated from $[\text{OD}(\text{without inhibitor}) - \text{OD}(\text{with inhibitor})] / [\text{OD}(\text{without inhibitor}) - \text{OD}(\text{background})] * 100$. The IC₅₀ value of each inhibitor was fit by GraphPad Prism 5.0 software.

3.7. Cellular Uptake and Blocking Studies

To prepare the cellular uptake experiment, 1×10^5 HepG2 cells were inoculated in each well of a 24-well plate and incubated for 24 h in a 5% CO₂ atmosphere at 37°C. For the cellular uptake assay, 1 µCi of the labeled compound was added to each well and incubated at 37°C for specific times (15, 30, 45, 60, 75, 90, and 120 min). All media was then removed and the cells were washed with cold PBS (containing 0.2% BSA). The cells in each well were lysed with 1 M NaOH, the solution was collected and the radioactive counts were measured with a gamma counter. For the blocking study, 1 µCi of the labeled compound and 10^{-5} M Gefitinib inhibitor were simultaneously added to each well and incubated under the same conditions. Then, the cells were lysed and collected. The cellular uptake values of radiotracers are shown in terms of the percentage of the injection dose per microgram protein that the cell contained with a decay correction normalized as the mean ± SD (%ID/mg, n=4). The blocking

percentage (%) at the specific time was calculated as $[\text{CPM}(\text{without inhibitor}) - \text{CPM}(\text{with inhibitor})] / \text{CPM}(\text{without inhibitor}) * 100$. The cellular association figures of each labeled compound were drawn with GraphPad Prism 5.0 software.

3.8. Biodistribution in S180 Tumor-Bearing Mice

Female ICR mice with S180 tumors were used for biodistribution experiments. At first, ICR mice were inoculated with S180 tumor cells (approximately 5×10^6 cells) in saline solution in the left forelimb by means of a subcutaneous injection. The experiment was performed one week after the inoculation. Each tumor-bearing mouse was injected with 0.1 mL of radiotracer saline solution (approximately 5 μCi) by means of a tail vein injection and euthanized at 5, 15, 30, 60, or 120 min post-injection. Required organs and tissue were excised and collected quickly. Then, radioactive counts of all organs and tissue were measured with a gamma counter, and masses of organs and tissue were weighed with an electronic analysis balance. The standard uptake values (SUVs) of radiotracers in organs and tissue were shown in the form of the percentage of the injection dose per gram with decay correction normalized as the mean \pm SD (%ID/g, n=4). SUVs (%) were calculated via the formula $\text{SUV}(\text{organ or tissue}) = \text{CPM}(\text{organ or tissue}) / [\text{CPM}(1\% \text{ injection dose}) * \text{Mass}(\text{organ or tissue})] * 100$.

4. Conclusions

To summarize, we successfully synthesized four novel radiotracers with low lipophilicity. All inhibitors had specific binding affinities to EGFR that appeared to be dose-dependent in ELISA. Due to the replacement of the 4-anilino group, the affinities to EGFR-TK of all these inhibitors were weaker than that of Gefitinib. In the cellular uptake study, the two radiotracers [^{18}F]I and [^{18}F]III, which had relatively high lipophilicity, exhibited high cellular uptake in HepG2 cell lines. The blocking studies in HepG2 cell lines demonstrated

that they were specifically bound to EGFR as well. In the biodistribution study, [¹⁸F]I and [¹⁸F]III had relatively higher tumor uptake and better clearance rates in plasma than the other two radiotracers. Overall, [¹⁸F]I was the most potential radiotracer for tumor imaging. From this research, we also concluded that we should control the lipophilicity of the quinazoline radiotracer at a proper level. We should balance the relationship between the specific binding ability to the receptor and the clearance rate in non-target organs and tissue in vivo as well. These conclusions will guide our concept of radiotracer molecular design in future research. Furthermore, experiments and PET studies will be carried out to evaluate the potency of [¹⁸F]I and other radiotracers that appear to be promising tumor imaging radiotracers.

Acknowledgements

We acknowledge with thanks the financial support from the National Natural Science Foundation of China (No.21571021). We also appreciate the cyclotron operator teams at the PET center of Xuanwu Hospital and The General Hospital of the People's Liberation Army for their support and technical assistance with radionuclides.

Conflicts of Interest

The authors declare no conflicts of interest.

References

1. Tebbutt N, Pedersen MW, Johns TG. Targeting the ERBB family in cancer: couples therapy. *Nat Rev Cancer*. 2013; 13: 663.
2. Tan F, Wang Y, Yuan X, Ding L, Hu B, Zhang L, Zhou J, Shengtu J, Sun Y. Targeted therapy for non-small-cell lung cancer using EGFR-TKIs. *Chin J New Drugs*. 2011; 20: 1595.

3. Fry DW, Kraker AJ, McMichael A, Ambroso L, Nelson JM, Leopold WR, Connors RW, Bridges AJ. A specific inhibitor of the epidermal growth-factor receptor tyrosine kinase. *Science*. 1994; 265: 1093.
4. Lynch TJ, Bell DW, Sordella R, Gurubhagavatula S, Okimoto RA, Brannigan BW, Harris PL, Haserlat SM, Supko JG, Haluska FG, Louis DN, Christiani DC, Settleman J, Haber DA. Activating mutations in the epidermal growth factor receptor underlying responsiveness of non-small-cell lung cancer to gefitinib. *N Engl J Med*. 2004; 350: 2119.
5. Wakeling AE, Guy SP, Woodburn JR, Ashton SE, Curry BJ, Barker AJ, Gibson KH. ZD1839 (Iressa): An orally active inhibitor of epidermal growth factor signaling with potential for cancer therapy. *Cancer Res*. 2002; 62: 5749.
6. Morgan MA, Parsels LA, Kollar LE, Normolle DP, Maybaum J, Lawrence TS. Improving gemcitabine-mediated radiosensitization using molecularly targeted therapy: A review. *Clin Cancer Res*. 2008; 14: 5142.
7. Burris-III HA. Dual kinase inhibition in the treatment of breast cancer: Initial experience with the EGFR/ErbB-2 inhibitor lapatinib. *The Oncologist*. 2004; 9: 10.
8. Sos ML, Rode HB, Heynck S, Perfer M, Fischer F, Kluter S, Pawar VG, Reuter C, Heuckman JM, Weiss J, Ruddigkeit L, Rabiller M, Koker M, Simard JR, Getlik M, Yuza Y, Chen TH, Greulich H, Thomas RK, Rauh D. Chemogenomic profiling provides insights into the limited activity of irreversible EGFR inhibitors in tumor cells expressing the T790M EGFR resistance mutation. *Cancer Res*. 2010; 70: 868.
9. Sequist LV, Yang JH, Yamamoto N, O'Byrne K, Hirsh V. Phase III study of afatinib or cisplatin plus pemetrexed in patients with metastatic lung adenocarcinoma with EGFR mutations. *J Clin Oncol*. 2013; 31: 3327.
10. Wagner HN. A brief history of positron emission tomography (PET). *Semin Nucl Med*. 1998; 28: 213.
11. Bars DL. Fluoride-18 and medical imaging: Radiopharmaceuticals for positron emission tomography. *J Fluoro Chem*. 2006; 127: 1488.
12. Salem A, Charnley N, Price P. Clinical molecular imaging with positron emission tomography. *Eur J Cancer*. 2006; 42: 1720.
13. Avril N, Propper D. Functional PET imaging in cancer drug development. *Future Oncol*. 2007; 3: 215.
14. Buck AK, Herrmann K, Shen C, Dechow T, Schwaiger M, Wester HJ. Molecular imaging of proliferation in vivo: Positron emission tomography with [F-18]fluorothymidine. *Methods*. 2009; 48: 205.
15. Shields AF, Grierson JR, Dohmen BM, Machulla HJ, Stayanoff JC, Lawhorn-Crews JM. Imaging proliferation in vivo with [F-18]FLT and positron emission tomography. *Nat Med*. 1998; 4: 1334.
16. Wester HJ, Herz M, Weber W. Synthesis and radiopharmacology of O-(2-[¹⁸F]fluoroethyl)-L-tyrosine for tumor imaging. *J Nucl Med*. 1991; 40: 205.
17. Grunbaum Z, Freauff SJ, Krohn KA. Synthesis and characterization of congeners of misonidazole for imaging hypoxia. *J Nucl Med*. 1987; 28: 68.
18. Vasdev N, Dorff PN, O'Neil JP, Chin FT, Hanrahan S, VanBrocklin HF. Metabolic stability of 6,7-dialkoxy-4-(2-, 3- and 4-[F-18]fluoroanilino)quinazolines, potential EGFR imaging probes. *Bioorg Med Chem*. 2011; 19: 2959.
19. Wang J, Gao M, Miller KD, Sledge GW, Zheng Q. Synthesis of [11C]Iressa as a new potential PET cancer imaging agent for epidermal growth factor receptor tyrosine kinase. *Bioorg Med Chem Lett*. 2006; 16: 4102.
20. Slobbe P, Windhorst AD, Walsum MS, Smit EF, Niessen HG, Solca F, Stehle G, Dongen G, Poot AJ. A comparative PET imaging study with the reversible and irreversible EGFR tyrosine kinase inhibitors [11C]erlotinib and [18F]afatinib in lung cancer-bearing mice. *EJNMMI Res*. 2015; 5: 14.
21. DeJesus OT, Murali D, Flores LG, Converse AK, Dick DW, Oakes TR, Roberts AD, Nickles RJ. Synthesis of [F-18]-ZD1839 as a PET imaging agent for epidermal growth factor receptors. *J Labelled Compd Rad*. 2003; 46: S1.

-
22. Murali D, Flores LG, Converse AK, Bartlett RM, Barnhart TE, Armstrong EA, Nickles RJ, Harari PM, DeJesus OT. Evaluation of [F-18]Iressa as a PET imaging agent for tumors overexpressing epidermal growth factor (EGF) receptor. *J Labelled Compd Rad.* 2005; 48: S294.
23. Seimbille Y, Phelps ME, Czernin J, Silverman DHS. Fluorine-18 labeling of 6,7-disubstituted anilinoquinazoline derivatives for positron emission tomography (PET) imaging of tyrosine kinase receptors: Synthesis of 18F-Iressa and related molecular probes. *J Labelled Compd Radiopharm.* 2005; 48: 829.
24. Su H, Seimbille Y, Ferl GZ, Bodenstein C, Fueger B, Kim KJ, Hsu YT, Dubinett SM, Phelps ME, Czernin J, Weber WA. Evaluation of [18F]gefitinib as a molecular imaging probe for the assessment of the epidermal growth factor receptor status in malignant tumors. *Eur J Nucl Med Mol Imaging.* 2008; 35: 1089.
25. Li S, Wang X, He Y, Zhao M, Chen Y, Xu J, Feng M, Chang J, Ning H, Qi C. Design and synthesis of novel quinazoline nitrogen mustard derivatives as potential therapeutic agents for cancer. *Eur J Med Chem.* 2013; 67: 293.

Accepted Article